



Model results for the ionospheric E region: solar and seasonal changes

J. E. Titheridge

► To cite this version:

J. E. Titheridge. Model results for the ionospheric E region: solar and seasonal changes. *Annales Geophysicae*, 1997, 15 (1), pp.63-78. hal-00316178

HAL Id: hal-00316178

<https://hal.science/hal-00316178>

Submitted on 1 Jan 1997

HAL is a multi-disciplinary open access archive for the deposit and dissemination of scientific research documents, whether they are published or not. The documents may come from teaching and research institutions in France or abroad, or from public or private research centers.

L'archive ouverte pluridisciplinaire **HAL**, est destinée au dépôt et à la diffusion de documents scientifiques de niveau recherche, publiés ou non, émanant des établissements d'enseignement et de recherche français ou étrangers, des laboratoires publics ou privés.

Model results for the ionospheric E region: solar and seasonal changes

J. E. Titheridge

Institute for Meteorology & Geophysics, University of Graz, Halbärthgasse 1, A-8010 Graz, Austria*

Received: 22 January 1996/Revised: 26 June 1996/Accepted: 22 July 1996

Abstract. A new, empirical model for NO densities is developed, to include physically reasonable variations with local time, season, latitude and solar cycle. Model calculations making full allowance for secondary production, and ionising radiations at wavelengths down to 25 Å, then give values for the peak density N_mE that are only 6% below the empirical IRI values for summer conditions at solar minimum. At solar maximum the difference increases to 16%. Solar-cycle changes in the EUVAC radiation model seem insufficient to explain the observed changes in N_mE , with any reasonable modifications to current atmospheric constants. Hinteregger radiations give the correct change, with results that are just 2% below the IRI values throughout the solar cycle, but give too little ionisation in the E-F valley region. To match the observed solar increase in N_mE , the high-flux reference spectrum in the EUVAC model needs an overall increase of about 20% (or 33% if the change is confined to the less well defined radiations at $\lambda < 150$ Å). Observed values of N_mE show a seasonal anomaly, at mid-latitudes, with densities about 10% higher in winter than in summer (for a constant solar zenith angle). Composition changes in the MSIS86 atmospheric model produce a summer-to-winter change in N_mE of about –2% in the northern hemisphere, and +3% in the southern hemisphere. Seasonal changes in NO produce an additional increase of about 5% in winter, near solar minimum, to give an overall seasonal anomaly of 8% in the southern hemisphere. Near solar maximum, reported NO densities suggest a much smaller seasonal change that is insufficient to produce any winter increase in N_mE . Other mechanisms, such as the effects of winds or electric fields, seem inadequate to explain the observed change in N_mE . It therefore seems possible that current satellite data may underestimate the mean seasonal variation in NO near solar maximum. A not unreasonable change in the data, to give the same 2:1 variation as at solar minimum, can produce a seasonal

anomaly in N_mE that accounts for 35–70% of the observed effect at all times.

1 Introduction

In recent years it has become possible to model, with reasonable accuracy, most of the processes involved in the formation of the ionosphere. The physics involved is particularly straightforward for the ionospheric E region, where the ionisation time-constant is only a few minutes, so that conditions are always close to equilibrium. Movement effects are also small, because of the short time-constants, so that changes due to diffusion, winds and electric fields are of minor importance. Model calculations are then reasonably straightforward. Results obtained for the peak density N_mE are, however, commonly about 30% below observed values, while the calculated width and depth of the valley between the E and F1 regions are perhaps two times too large (e.g. Titheridge, 1990; Buonsanto, 1990; Buonsanto *et al.*, 1992; Tobiska, 1993). Because of the square-law loss process, an increase of 40% in N_mE requires an increase of 100% in the ionisation rate at the peak of the E layer (at 105–110 km). To reduce the size and depth of the valley requires an even larger increase in production at heights of 120–150 km.

In a previous paper (Titheridge, 1996), production rates were calculated using a new approach to determine the total amount of secondary ionisation, based directly on the energy of the incoming photons. This procedure automatically makes full allowance for changes in the EUV spectrum and in the photo ionisation cross-sections. It gives an increase of up to 20% in values of N_mE calculated using the newer radiation models which have increased fluxes at short wavelengths. The EUV models commonly used for ionospheric calculations extend down to a wavelength of 50 Å, with all radiations between 50–100 Å included in a single band. Subdividing this band, and including radiations down to 25 Å, gives a further increase of 8–10% in N_mE , so that final values are now only 12% below mean experimental results for equinox conditions at $F_{10.7} = 110$.

* Permanent address: Physics Department, The University of Auckland, Auckland, New Zealand
Correspondence to: J. E. Titheridge

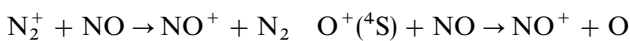
Ionospheric models are particularly valuable for investigating the changes that would result, in observed quantities, from changes in individual input parameters. In the present work a study is made of the changes in N_mE with season and with solar cycle, caused by changes in current models of the solar EUV radiation and in the composition of the neutral atmosphere. For this purpose, a new model for the density of NO in the upper atmosphere is described. This uses recent data from the Solar Mesosphere Explorer (SME) satellite to construct an empirical model that has reasonable variations with season, latitude, solar cycle and time of day. NO is produced by solar radiation, giving increased densities in summer that lead to an increase in loss rates for O_2^+ ions in the E region. It therefore seemed that changes in NO might explain some of the observed seasonal anomaly in the E region – where values of N_mE are about 10% larger in winter than in summer, for mid-latitude conditions at a constant solar zenith angle.

Model calculations are also used to see whether the solar variations in current EUV flux models are compatible with observed changes in the ionosphere. For this purpose we assume that solar-cycle changes in the neutral atmosphere are correctly defined by the MSIS86 atmospheric model (Hedin, 1987). Results suggest that, even if the normal increase of NO near solar maximum is suppressed, the EUVAC model as it stands cannot give a sufficiently fast increase in E-region densities during the solar cycle. The earlier Hinteregger model, however, gives a rate of change that closely matches the observations.

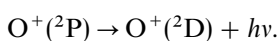
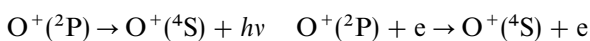
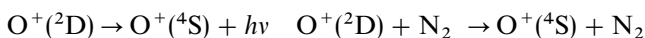
For comparisons with experimental data, use is made of results incorporated in the International Reference Ionosphere model IRI-90 (Bilitza, 1990). This model uses analytic expressions that have been fitted to a large amount of monthly median data, to best reproduce mean observed values of ion density at different heights. In particular, it gives values of N_mE corresponding to the results obtained by Kouris and Muggleton (1973a, b) from an extended study of monthly median values of foE, for each hour between 0900 and 1500, from 45 sites spaced around the globe, and covering a full 11-year solar cycle.

2 The modelling program

The general features of the modelling program have been described previously (Titheridge, 1993). The densities of O, O_2 , N, N_2 and H are obtained from the MSIS86 atmospheric model (Hedin, 1987). Ion chemistry includes all the reactions normally considered (e.g. Buonsanto *et al.*, 1992) plus four further charge-exchange reactions involving NO:



and five metastable decay processes:



Allowance is made for the direct production of N^+ ions, through ionisation of N_2 or of N, since this is significant under some conditions. H^+ calculations are included, along with a full allowance for the effects of diffusion, winds, exospheric fluxes and temperature gradients (as summarised by Titheridge, 1993) to ensure a realistic F-layer as the upper bound of the valley region.

The total number of ions that are produced by one photon depends mainly on the energy of the photon. This dependence has been used to construct a simple scheme for obtaining a close approximation to the total ion production under a wide variety of conditions (Titheridge, 1996). Unlike traditional methods, which determine the bidirectional photoelectron flux as a function of height, calculations based on the overall energy distribution work well at all heights down through the lower E region. Compared with earlier calculations using a fixed correction of 30%, inclusion of a full allowance for secondary production gives an increase of about 20% in calculated densities at the peak of the E-layer. The increase is even larger at heights above the peak of the layer, so that the size of the E-F1 valley is appreciably reduced.

For most calculations EUV intensities are taken from the recent EUVAC model (Richards *et al.*, 1994), which uses linear interpolation between reference spectra at $F_{10.7} = 80$ and 200. The intensities are specified in 37 wavelength bands covering the range from 50 to 1050 Å, as used in many studies (e.g. Torr and Torr, 1985). In the present work two changes are made to this scheme. Firstly, the normal band 1 (from 50–100 Å) is divided into smaller sections. This is necessary for accurate profile calculations at heights below 150 km, because of the large number of secondary electrons produced by high-energy photons. As the wavelength decreases from 100 to 50 Å, the mean number of secondary ions produced per photon increases from about 2.1 to 4.4, while the height of maximum production decreases by about 9 km (Titheridge, 1996). To reproduce these changes correctly, and to include the secondary ionisation produced by high-energy photons in the range 25–50 Å, the normal band 1 is replaced by four bands covering 25–40, 40–60, 60–80 and 80–100 Å. Photoionisation cross-sections for these bands are obtained from the detailed data of Fenelly and Torr (1992), as described in Titheridge (1996).

The second change to the commonly used EUV spectrum is the addition of a band to include the strong Ly α radiation at 1216 Å. This radiation produces NO^+ ions only, and is the major source of ionisation at heights below 95 km. Direct ionisation of NO by Ly α also increases total ionisation rates by about 2% in the daytime E region. At night, scattered Ly α provides up to 30% of the total ionisation at heights near 130 km.

3 An empirical model for the NO layer

3.1 The production and loss of NO

At low and mid-latitudes, NO is produced primarily as a result of daytime photoionisation. Direct or indirect dissociation of N_2 , by solar photons and secondary

electrons, produces excited $N(^2D)$ atoms which react with O_2 to produce NO. The normal ground state $N(^4S)$ can also produce NO, but the rate constant for this reaction is slower by a factor of over 10000 at heights below 120 km (Rusch *et al.*, 1991; Torr *et al.*, 1995). So in the E region, production of NO is important only during the day.

Loss of NO is mainly through its reaction with $N(^4S)$, particularly at night when the densities of $N(^2D)$ and O_2^+ are greatly reduced (e.g. Torr *et al.*, 1995). In the E and F1 regions the density of $N(^4S)$ increases with height, giving increasing loss rates. This produces a well-defined NO layer with a peak near 110 km. We should note that $N(^4S)$ densities are not well defined at heights below 200 km, where data are very sparse and the variations in the MSIS86 model are guided largely by theory. Theoretical calculations of NO densities based on this data do, however, provide a good match with AE-C measurements over the height range 130–250 km (Rusch *et al.*, 1991).

At 120 km the density of $N(^4S)$ is about $2.0 \times 10^6 \text{ cm}^{-3}$ near noon, giving a time-constant of 4 h for the loss of NO. The time-constant drops to 1.6 h at a height of 130 km, and 0.8 h at 140 km, as the density of $N(^4S)$ increases (with a peak near 190 km). $N(^4S)$ densities are approximately halved at night, causing the time-constants to increase by a factor of about 2 after midnight. Night-time recombination with a mean time-constant of around 6 h (at 120 km) should cause NO densities to decrease by a factor of 5–10, reaching a minimum just before dawn. Mean daytime densities should follow the latitudinal, seasonal and solar-cycle changes in the solar irradiance, at low and mid-latitudes. Current results suggest an increase by a factor of about 2 from winter to summer, at latitudes of 25° – 40° near solar minimum (e.g. Stewart and Cravens, 1978; Gérard and Noël, 1986). This is sufficient to make appreciable changes to the E-region ionisation.

At high latitudes there is a large production of $N(^2D)$ by electron impact in the auroral regions. The resulting production of NO is larger and more variable than at low latitudes, with little diurnal variation and only a small solar-cycle change. NO densities will increase, and extend to lower latitudes, with increases in magnetic activity; this could have produced the apparent increase in mid-latitude densities in winter, found in some early studies. Even under quiet conditions the data of Fesen *et al.* (1990) show day-to-day variations of up to about $\pm 20\%$ in NO densities at latitudes below 45° , and twice this at higher latitudes.

3.2 Daytime densities, as a function of solar activity

Published studies suggest that from solar minimum to solar maximum the daytime NO densities, at low latitudes, increase by a factor of about 3.5 (Kuze and Ogawa, 1988; Gérard *et al.*, 1993); 3–4 (Gérard *et al.*, 1990); 4–5 (Fesen *et al.*, 1990); 7 (Fuller-Rowell, 1993); and 7.5 (Barth *et al.*, 1988). Seasonal and latitudinal variations, in the daytime thermosphere, are shown best in the work of Fesen *et al.* (1990). This uses data from the Solar Mesosphere Explorer satellite at local times near 1500 LT, close to the diurnal maximum in NO. Mean variations

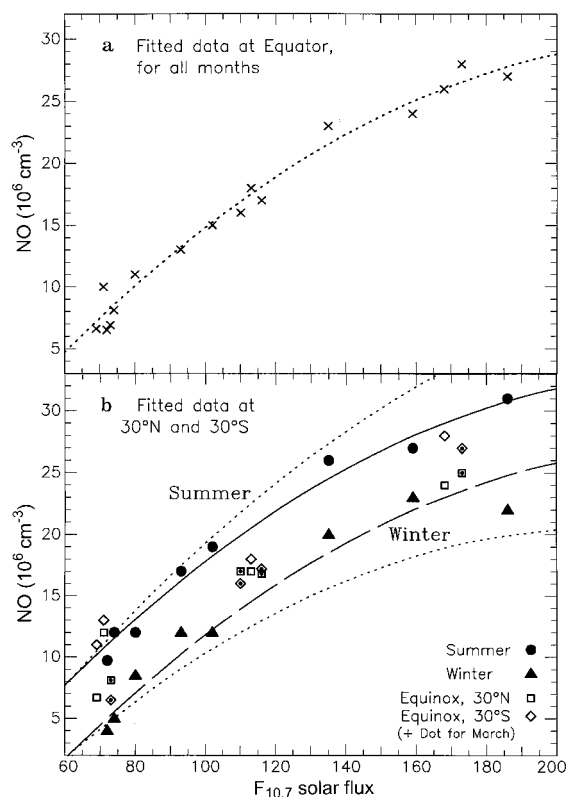


Fig. 1a, b. Mean values of NO **a** at the equator and **b** at latitudes of $30^\circ N$ and $30^\circ S$, for the months of March, June, September and December of each year from 1982 to 1985. Each point gives a mean value for the peak density, at heights near 110 km and for a local time near 1500 LT, from Fesen *et al.* (1990). All data are for magnetically quiet conditions. The plotted curves are obtained from Eq. 2. Dotted lines in **b** show a modified variation discussed in Sect. 6

with latitude are given for March, June, September and December of each year from 1982 to 1985, covering solar fluxes from about 180 to 70. Mean values for the peak density of NO, at the height of the maximum (near 110 km), are also tabulated for each month and each year at latitudes of 0° , $\pm 30^\circ$ and $\pm 60^\circ$.

The 16 mean values given by Fesen *et al.* (1990), at 0° latitude, are plotted in Fig. 1a. The data show a well-defined increase with solar activity, by a factor of about 4, for values of $F_{10.7}$ increasing from 69 to 186. There is no consistent variation with month, and all data show some tendency for a decrease in $\Delta(\text{NO})/(\Delta F_{10.7})$ near solar maximum. The mean trend is well represented by the dotted line in Fig. 1a, which corresponds to the relation

$$D' = 14.8 + 0.22(F_{10.7} - 100) - 0.0008(F_{10.7} - 100)^2 \times 10^6 \text{ cm}^{-3}. \quad (1)$$

The most recent low-latitude data set is that used by Gérard *et al.* (1993) for comparison with model calculations. These data tend to be grouped near solar fluxes of about 73, 105 and 170. Mean values were scaled for each group, giving NO densities of $8.5(8.3)$, $16(15.9)$ and $28(26) \times 10^6 \text{ cm}^{-3}$. Values in brackets are the corresponding results from Eq. 1. The good agreement lends confidence in

the use of Eq. 1 to define the mean density at the peak of the NO layer, at low latitudes.

3.3 Seasonal and latitudinal changes

The mean values of NO density tabulated by Fesen *et al.* (1990), for latitudes of 30°N and 30°S, are plotted in Fig. 1b. Solid dots are for the summer hemisphere, and solid triangles for winter; these include all the tabulated data for June and December. Two points (at 30°S, in June 1984 and 1985) have been adjusted downwards, since they fall on the start of the rising portion of the mean plots, where the winter values increase rapidly towards the higher auroral density (as will be discussed). The winter value at $F_{10.7} = 186$ has also been adjusted upwards by 10%. These changes give points that follow more accurately the trend of the central near-linear section of the mean plots in Fesen *et al.* (1990).

The mean summer and winter densities plotted in Fig. 1b, for a latitude of 30°, show an overall trend that is very similar to the equatorial results of Fig. 1a. The continuous and broken lines correspond to the dotted curve in Fig. 1a, shifted by $\pm 3.0 \times 10^6$. This provides a near-optimum fit to the data for both summer (solid dots) and winter (triangles). The equinox data from Fesen *et al.*, for March and September of each year, are shown as open symbols. These are coded according to the hemisphere, with values for March distinguished by a central dot. At medium and high levels of solar activity these equinox data (at a latitude of 30°) are reasonably well centred between the summer and winter curves. Thus they agree well with the curve of Fig. 1a, based on data from March, June, September and December at a latitude of 0°. The agreement is less good near solar minimum, but still acceptable in view of the increased scatter at this time.

The fixed difference between the three plotted curves in Fig. 1 corresponds to a fixed latitudinal gradient in the NO densities, of 0.10×10^6 per degree of latitude, for summer or winter. The lack of any consistent variation with month or with latitude in the equinox data (open symbols in Fig. 1b), indicates a mean gradient of zero between 30°N and 30°S for the equinox months. The combined latitudinal and seasonal change can therefore be represented by the relation

$$D_0 = 14.8 + 0.22(F_{10.7} - 100) - 0.0008(F_{10.7} - 100)^2 + 0.1s \cdot \phi \times 10^6 \text{ cm}^{-3}, \quad (2)$$

where ϕ is the latitude in degrees; s is a seasonal index which varies from +1 in June to 0 at the equinoxes and -1 in December, so that $s = \sin(0.0172[d - 80])$, where d is the day number. The seasonal term gives a constant change from winter to summer, so that the summer/winter ratio is greatly reduced near solar maximum. As discussed in Sect. 6, this does not agree well with simple physical considerations or with observed seasonal changes in $N_m E$, and a modified form giving a constant seasonal effect might be preferable. This is obtained using Eq. 14 in place of Eq. 2, and gives the variations shown by dotted lines in Fig. 1b.

Scatter plots were also given by Fesen *et al.* (1990) for data in two quiet periods in each of June and December. Mean trend lines drawn through these four sets give slopes (at the equator) of 0.10, 0.09, 0.08 and $0.08 \times 10^6 \text{ cm}^{-3}$ per deg latitude. The consistency of these results, in spite of a 2:1 variation in the equatorial densities, supports the use of a fixed latitudinal gradient. The restriction to quiet intervals has produced a slightly lower gradient than the value (0.1×10^6) obtained from the overall mean plots, but the change is barely significant. The different plots in Fesen *et al.* (1990) show that this approximately constant gradient is observed, in most cases, at latitudes from about 30° in the winter hemisphere to 60° in summer.

3.4 A high-latitude model

In the auroral regions there is a large, additional source of NO from high-energy particle precipitation. The mean curves given by Fesen *et al.* show increased NO densities at latitudes above 60°, with a tendency to peak at about 75° (as also found by Gérard *et al.*, 1990). For latitudes of 60°–90° most of the mean data lie between 20 and 40×10^6 , in all years and all seasons. There is some dependence on solar activity, with mean values increasing from about 22 at $F_{10.7} = 70$ to 33 at $F_{10.7} = 180$ giving

$$D_F = (15 + 0.1F_{10.7}) \times 10^6 \text{ cm}^{-3}. \quad (3)$$

Smith *et al.* (1993) used data from 51 rocket flights and 36 satellite sets, to determine the mean variation of NO density with latitude, exospheric temperature and K_p . The data were primarily from latitudes near 0, 31, 39 and 60–65°N, at values of $F_{10.7}$ from about 70–250. For the high-latitude group there was little diurnal variation, but a large change with magnetic activity. The changes with K_p corresponded to a factor $\exp(0.40K_p)$ for the rocket data, and $\exp(0.26K_p)$ for the satellite results. We will assume a mean K_p variation corresponding to $\exp(0.32K_p)$. For values of K_p up to about 5, this can be approximated quite well by a term $(1 + 0.1A_p)$, where A_p is the planetary index.

The changes with solar activity were given as a factor $\exp(c_1 T_\infty)$, where T_∞ is the exospheric temperature and $c_1 = 0.0010$ for the rocket data and 0.0005 for the satellite results. From the tables in Smith *et al.* we have $T_\infty \approx 4F_{10.7} + 525$ for these data. Using $c_1 = 0.0008$ then gives a solar-cycle change proportional to $\exp(0.0032F_{10.7})$, so that NO densities increase by 52% when $F_{10.7}$ changes from 100 to 230. This agrees very closely with the variation D_F derived from the work of Fesen *et al.* (1990), as shown in Fig. 2. The NO variations at high latitude are therefore defined by

$$D_H = 0.5(15 + 0.1F_{10.7})(1 + 0.1A_p) \times 10^6 \text{ cm}^{-3}. \quad (4)$$

The Fesen *et al.* data correspond to a median A_p of 17, so that Eq. 4 requires an initial constant of 0.37 to agree with Eq. 3. The Smith *et al.* data give appreciably greater NO densities, corresponding to an initial factor 0.66. The value 0.5 used in Eq. 4 is close to the geometric mean of

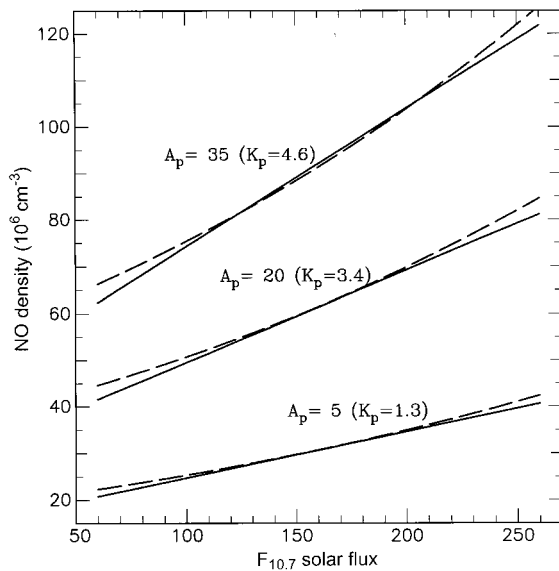


Fig. 2. Mean values for the peak NO density, at latitudes of 60–90°, as a function of solar flux and magnetic activity. *Solid lines* are from Eq. 4; this corresponds to the mean high-latitude results of Fesen *et al.* (1990) (at $A_p \approx 17$) increased by 35%. *Broken lines* give the expression $D_{NO} = \exp(15.91 + 0.0032F_{10.7} + 0.005K_p)$, derived from the work of Smith *et al.* (1993), decreased by 24%

these estimates. This high-latitude result is used to define the density at the peak of the daytime NO layer, for latitudes greater than 60° in both hemispheres.

Optimum agreement with the full set of plots given by Fesen *et al.* (1990) is obtained if Eq. 2 is used for latitudes of -45° to $+45^\circ$ in March, -30° to $+50^\circ$ in June, -20° to $+40^\circ$ in September and -50° to $+30^\circ$ in December. Results then reproduce, for instance, the steady increase in [NO] from -20° to -60° evident in all four of the September data sets. The present study adopts a slightly simpler procedure, with upper limits of 40° for both hemispheres in March and September. Equation 2 is then used up to a latitude ϕ_M of 30° in winter, 40° in equinox and 50° in summer, given by

$$\phi_M = 40 + 10 \cdot s \text{ degrees}, \quad (5)$$

where s is the seasonal index from Eq. 2. This gives a symmetrical mean variation for determining average global changes.

At latitudes above 60°, peak densities are defined by Eq. 4. Intermediate latitudes use a linear interpolation between the results from Eq. 2, at a latitude ϕ_M , and the results from Eq. 4 for a latitude of 60°. This interpolation is quite smooth in summer, when Eqs. 2 and 4 give similar results at $\phi \approx 60^\circ$. A much larger change is involved in winter, when the data (and the change from Eq. 2 to Eq. 4) give an increase by a factor of 1.2 to 4 over a latitude range from about 30° to 60°.

3.5 Diurnal variations

Good data on the diurnal variations in NO densities are not readily available, since most satellite measurements

are restricted to daylight hours. To overcome this problem, Smith *et al.* (1993) analyse seven rocket and six satellite values for the density at a height of 110 km. Results at the equator show an increase by a factor of 7 from the predawn minimum to the mean daytime value. This factor decreased at higher latitudes, or with increases in K_p . For a latitude of 30°, and $K_p = 2.5$, the derived expressions give a mean day/night ratio of only 2–3. This value is supported directly by only a small number of mid-latitude rocket data, which give a mean diurnal variation of about 3:1. The decrease with latitude seems to be caused primarily by the inclusion of data at latitudes above 60° in an overall, linear correlation. The high-latitude data (clustered near 65°) show no significant diurnal variation, but a high correlation with K_p – whereas the low-latitude data show a large diurnal change and no correlation with K_p .

Changes in the density at the peak of the NO layer, from 0600 to 1800 LT at the equinoxes, are clearly displayed in the results of Rusch *et al.* (1991). Data from the satellite Atmosphere Explorer C, at latitudes of 0°–30°, are compared with the results of a full model calculation. In both cases there is a rapid increase of NO densities from 0600 to 1000, with maximum values occurring at about 1400. For the satellite data, the increase from 0600–1400 was by a factor of 6.5 at a height of 160 km, and a factor of 10 at the lower limit of observations (135 km). Model results show a slightly smaller increase, corresponding to a factor of 5 at 160 km and a factor of 6.5 at heights near the peak (about 120 km). These changes are in reasonable agreement with the increase by a factor of 7 at the height of peak density (near 110 km) found by Smith *et al.* (1993).

For the present work the diurnal variation at latitudes up to ϕ_M is modelled by the relation

$$V_a = 0.535 - 0.465 \cdot \cos(H_T - 0.7 - 0.5 \cdot \sin[H_T - 0.2]), \quad (6)$$

where H_T is the hour angle in radians ($= 0.262 T$, where T is the local time in h). This expression gives a rapid rise after 0600, and a slower, near-exponential decay at night. To increase the length of the daytime interval in summer and equinox, Eq. 6 is scaled up by a factor S_V , and the peak flattened, using the relation

$$V = S_V / (V_a^{-2} + S_V^2 - 1)^{0.5}. \quad (7a)$$

The scale factor S_V is a function of latitude and season, given by

$$S_V = 1.40 + 0.0172(s \cdot \phi) + 0.0028 \cdot |\phi|. \quad (7b)$$

The value V obtained from Eq. 7 is used as a multiplying factor for the maximum daytime density D_o (Eq. 2), giving the final result for the density at the peak of the NO layer as

$$D_p = D_o V. \quad (8)$$

The function V gives a good approximation to the required diurnal shape near equinox, with a minimum (0.1) at 0420 and a maximum (1.0) at 1400 LT. Densities increase rapidly from 0500–1100, by a factor of 7.7. From

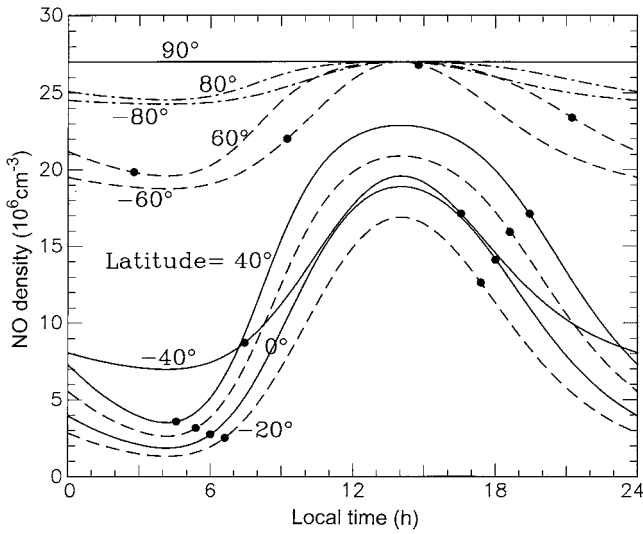


Fig. 3. Model values for the density at the peak of the NO layer, for June solstice conditions at $F_{10.7} = 120$ and $A_p = 10$. Solid dots mark the times of sunrise and sunset

0600 to 1400 the NO density increases by a factor of 7. This is a compromise between the experimental results of Rusch *et al.* (1991), which suggest a factor of 10, and their theoretical model, which gives a factor of 6. At sunset the NO density is 25% less than the diurnal maximum (for latitudes up to $\pm 40^\circ$, as in Fig. 3). The night-time variation, from 1900 to 0300, gives a near-exponential decay with a time-constant of about 5 h.

At latitudes above 60° the diurnal variation is reduced in accordance with the results referenced in Sect. 3.4. For a latitude of 90° the density at the peak of the NO layer is assumed constant at the value D_H (Eq. 4). The diurnal variation is increased linearly at decreasing latitudes, giving a change at 60° that is one-third of the variation at low latitudes. Thus for ϕ in the range 60° – 90° we use

$$D_p = D_H(\phi/90 + V(1 - \phi/90)). \quad (9)$$

For latitudes in the range ϕ_M to 60° , results are obtained by linear interpolation between the densities at these end points. A simple FORTRAN routine that carries out these calculations can be obtained from the author (email to j.titheridge@auckland.ac.nz).

Diurnal variations in NO densities, calculated as above, are shown in Fig. 3. These curves are for June solstice conditions, with $F_{10.7} = 120$, at latitudes from 80°N to 80°S in steps of 20° and at the poles. With the globally symmetrical model, results apply equally well to the seasonal changes at a given site (apart from a small effect due to the last term in Eq. 7b). Thus the three solid-line curves labelled 40° , 0° and -40° also show the changes at a latitude of 40°N for summer, equinox and winter. Sunrise and sunset times at the different latitudes (or different seasons) are marked by solid dots in Fig. 3. These results should provide a reasonable first-order representation of likely changes in NO densities, at heights near 110 km, until more detailed observations are available.

3.6 Changes with height

The height variation of the NO density will be approximated by an α -Chapman layer. This has a slightly sharper peak than the β -Chapman layer, agreeing better with most published curves, and gives

$$D(h) = D_p \exp \{0.5(1 - z - \exp[-z])\}, \quad (10)$$

where $D_p = D_0 V$, and $z = (h - h_p)/H_{\text{NO}}$; h_p is the height of the peak density of NO, and H_{NO} is the assumed scale height (about 0.7 times that for a β -Chapman layer of similar thickness).

Vertical profiles tabulated by Barth (1990) show the peak density occurring at a mean height of 110 km. Gérard and Noël (1986) give AE-D data for December, solar minimum, as a function of height and latitude. This shows h_p increasing from about 106 km at 30°N to 110 km at 40°S . This corresponds to $h_p = 108 + 0.06(s \cdot \phi)$, where $(s \cdot \phi)$ gives the latitude in degrees, positive in summer, as in Eq. 2. Data from the SME satellite are shown as a function of height and of latitude by Gérard *et al.* (1990). Values of h_p from these data show a change from about 110 km at -45° to 112 km at $+45^\circ$, in June. There is no overall increase with solar flux, from $F_{10.7} = 79$ to 172, suggesting a variation $h_p = 111 + 0.02(s \cdot \phi)$.

Gérard *et al.* (1990) also give model results for the daytime NO density as a function of height and latitude, for June solstice conditions at $F_{10.7} = 80$ and 200. These densities are dependent on assumed values for several constants, in particular the eddy diffusion coefficients (Fesen *et al.*, 1990), which could change the peak heights. The model results show h_p increasing in the summer hemisphere, and an increase with $F_{10.7}$ which can be represented approximately by $h_p = 109 + 0.01 \cdot F_{10.7} + 0.05(s \cdot \phi)$. Model calculations by Gérard *et al.* (1993) give $h_p = 111$ km, for values of $F_{10.7}$ from 70 to 240.

As a compromise between these results we will use the expression

$$h_p = 110 + 0.005F_{10.7} + 0.04(s \cdot \phi) \text{ km}. \quad (11)$$

This gives a winter to summer variation of 2–3 km at mid-latitudes, and an increase of 1 km at solar maximum. Calculations and data from the AE-C satellite (Rusch *et al.*, 1991) show a significant diurnal variation of h_p , with an increase of 10–20 km for a few hours after sunrise, but the data are available only at heights above 135 km so the peaks are not fully defined.

Data from the AE-D satellite (Gérard and Noël, 1986) show height variations corresponding to a scale height $H_{\text{NO}} \approx 5$ –8 km near solar minimum. Contour plots of SME data (Gérard *et al.*, 1990) give vertical scale heights of 7.5 and 8 km at $F_{10.7} = 79$ and 172. Corresponding model results have $H_{\text{NO}} \approx 10$ at $F_{10.7} = 80$, and 11.8 km at $F_{10.7} = 200$. Profiles calculated by Siskind and Rusch (1992) correspond to a scale height of 6–7 km at $F_{10.7} \approx 260$. Smith *et al.* (1993) show an average of the mean profiles tabulated by Barth (1990) for different conditions, including solar minimum and maximum; this profile corresponds to $H_{\text{NO}} \approx 8$ km. Solar minimum data

from the AE-C satellite, and corresponding model calculations (Rusch *et al.*, 1991), both indicate $H_{\text{NO}} \approx 9$ km. Gérard *et al.* (1993) also give model results which indicate $H_{\text{NO}} \approx 9$ km, with no clear variation with solar flux. From these data it seems reasonable to use a scale height increasing from about 8 to 9 km over the solar cycle, given by

$$H_{\text{NO}} = 8 + 0.005F_{10.7} \text{ km.} \quad (12)$$

4 Calculated profiles

4.1 Ion composition

Ion composition results for typical summer day conditions are shown in Fig. 4. These are calculated using the EUVAC radiations and current values for the photo-ionisation cross-sections, as described in Sect. 2, with a full allowance for secondary ionisation. N_2^+ is the main ion produced at heights of 110–190 km, but this converts rapidly to NO^+ (with about 10% to O^+ and O_2^+) at heights below 170 km. Direct production of NO^+ from NO is very small, for zenith angles less than 80° , but indirect production causes NO^+ to be the major ion from about 125–180 km. Ignoring the effect of NO in the atmosphere gives ion densities shown by the fine lines in Fig. 4, with NO^+ predominating only down to 140 km. Under these conditions the loss of O_2^+ by conversion to NO^+ is appreciably reduced at heights below 150 km. Since the recombination coefficient for O_2^+ is only half as large as for NO^+ , this gives a reduced overall loss rate and an increase of 9% in N_mE .

Figure 4 highlights a continuing problem in current models of the E region. Ion composition measurements from rockets indicate that NO^+ is the major ion near the peak of the E-layer (Keneshea *et al.*, 1970; Danilov and Semenov, 1978; Swider and Keneshea, 1993). Most modelling calculations show that NO^+ becomes less important than O_2^+ at heights below 130–140 km, as discussed by Buonsanto *et al.* (1995). Results from the present model, with the improvements described in Sect. 2, do slightly better – giving a transition from NO^+ to O_2^+ at a height near 120 km, for medium levels of solar activity (as in Fig. 4 and Table 1b).

The rocket results of Keneshea *et al.* (1970) and Swider and Keneshea (1993) show the ratio NO^+/O_2^+ reaching a maximum at heights of 105–125 km, where the proportion of NO^+ reaches 94–98%. These data are, however, for conditions near sunrise and sunset, with zenith angles of 89° – 102° and $F_{10.7} = 140$. Model calculations for these conditions, using the normal 37 radiation bands (from 50–1050 Å), give $\text{NO}^+ < 90\%$ of N_e at all heights. The present work adds the strong Ly α line at 1216 Å, as described in Sect. 2. For twilight conditions, this radiation is absorbed in the E region giving a large production of NO^+ by direct ionisation of NO (as described by Swider and Keneshea). For zenith angles of 90° and 95° , at $F_{10.7} = 140$, the model calculations (shown in Table 1b) give a peak NO^+ proportion of about 96%, at a height of 110–130 km, in reasonable agreement with the above rocket data.

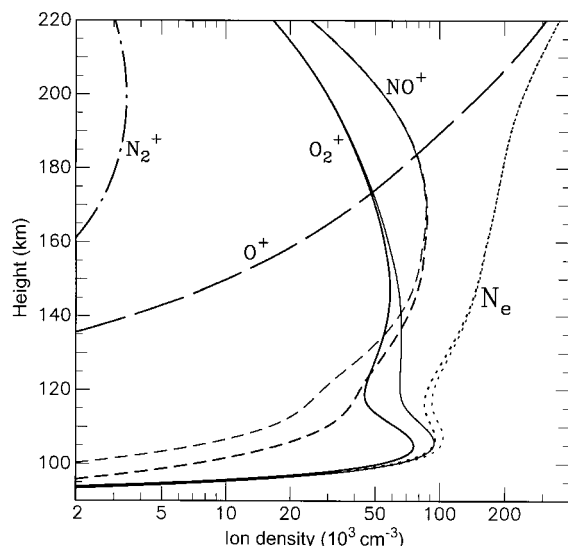


Fig. 4. Ion densities for summer conditions at 40°N , with $\chi = 60^\circ$ and $F_{10.7} = 100$. Fine lines show the results obtained if NO densities are reduced to zero

Mitra and Benerjee (1971) have also studied ion composition variations, using rocket data from six mid-latitude flights at $\chi = 50^\circ$ – 60° . Three flights were at low solar activity, with a mean value $F_{10.7} = 73$, while three flights were at high activity with a mean $F_{10.7} = 235$. Both sets had a mean zenith angle $\chi = 57^\circ$. The mean percentage of NO^+ ions obtained from these data are shown in italics in Table 1a and c. Bracketed values in Table 1b are obtained by linear interpolation in $F_{10.7}$. Agreement with the present model results is good at all levels of solar activity, and all available heights (from 120 to 200 km). At $F_{10.7} = 70$ and 140 the agreement is excellent at all heights from 160 km down to (and including) 120 km.

The most complete data on observed ion composition in the E region is given by Danilov and Semenov (1978), based on 43 rocket mass spectrometer measurements carried out at latitudes of 30° – 50°N . These data were combined and smoothed to produce tables giving the proportions of O^+ , O_2^+ and NO^+ ions at heights of 100 to 200 km, for summer, equinox and winter conditions, at seven zenith angles (from 20° to 90°) and two levels of solar activity ($F_{10.7} = 70$ and 140). Expressions fitted to these data are used for ion-composition calculations in the International Reference Ionosphere (Bilitza, 1990). The tabulated results for NO^+ ions, for equinox conditions at four zenith angles, are reproduced in Table 1 and compared with the present model calculations. For heights above 130 km the agreement is quite good, with the Model and Rocket results differing by less than a factor of 1.2 in most cases. Differences are larger and more variable near 200 km, because of changes in the rate of O^+ increase at the base of the F-layer.

The present NO model is best defined for equinox conditions, at low and mid-latitudes (from Fig. 1a). At $F_{10.7} = 140$, when the NO density is fairly large, the Model and Rocket results in Table 1b are in reasonable accord at heights down to 120 km. Agreement is also quite

Table 1. The percentage of NO⁺ ions at heights from 100 to 200 km, from the present Model calculations at a latitude of 40°N, and from mean Rocket results tabulated by Danilov and Semenov (1978). Values in italics are from rocket data analysed by Mitra and Benerjee (1971)

	Height	100	110	120	130	140	150	160	180	200 km
(a) $F_{10.7} = 70$										
$\chi = 40^\circ$	Model	7	23	35	45	50	51	48	33	13 %
	Rocket	36	49	55	56	56	53	49	37	17
$\chi = 57^\circ$	<i>Rocket</i>	–	–	37	41	46	49	48	25	12
	Model	9	22	37	43	49	51	49	34	13
$\chi = 60^\circ$	Rocket	47	54	58	56	56	53	49	37	17
	Model	46	23	39	47	48	51	54	39	15
$\chi = 80^\circ$	Rocket	66	66	65	63	58	54	52	40	22
	Model	53	81	50	50	58	66	67	58	17
$\chi = 90^\circ$	Rocket	91	81	76	74	66	63	63	54	34
(b) $F_{10.7} = 140$										
$\chi = 40^\circ$	Model	13	33	46	53	55	53	49	32	12 %
	Rocket	36	49	55	56	56	53	45	27	10
$\chi < 57^\circ$	<i>Rocket</i>	–	–	53	52	53	53	51	30	15 >
	Model	20	34	52	55	57	55	52	34	13
$\chi = 60^\circ$	Rocket	46	54	57	56	56	53	45	27	10
	Model	78	46	58	61	61	61	61	45	18
$\chi = 80^\circ$	Rocket	66	66	65	63	58	54	48	33	14
	Model	81	95	73	67	71	75	77	70	32
$\chi = 90^\circ$	Rocket	91	81	76	74	66	73	58	46	28
	Model	74	89	96	97	96	91	89	88	51
(c) $F_{10.7} = 235$										
$\chi = 57^\circ$	<i>Rocket</i>	–	–	77	67	62	59	56	39	20
	Model	24	36	58	62	63	62	57	38	19 %

good (at all heights) near sunrise and sunset, when Ly α radiation gives a large production of NO⁺ in the E region. At heights of 100–110 km, however, model results for the proportion of NO⁺ ions are commonly about half of that indicated by the rocket data at zenith angles up to 80°. The differences are largest at $F_{10.7} = 70$, due to the almost complete absence of any solar cycle change in the ‘Rocket’ results. This seems unrealistic, in view of the clear changes in NO density (Fig. 1a), and in the independent rocket data at $\chi = 57^\circ$ in Table 1. Thus the Rocket data at $F_{10.7} = 70$ may give NO⁺ ratios which are up to 50% too high at 120 km, for $\chi = 60^\circ$.

For $F_{10.7} = 140$, and $\chi \leq 80^\circ$, the comparison in Table 1b suggests that the model results are acceptable at heights down to about 120 km. At lower heights the calculated proportion of NO⁺ is less than the rocket results by a factor of 1.5 at 110 km, and a factor of about 2 at 100 km. The difference is caused by a rapid decrease in calculated NO⁺ densities, at heights below about 115 km, and the large increase in O₂⁺ production at the E-region peak near 108 km. N₂⁺ ionisation produced at these heights is converted almost entirely to NO⁺, with a rate constant about 1000 times greater than for the conversion of O₂⁺ to NO⁺. With our current understanding of E-region chemistry, this leaves four possibilities for increasing the proportion of NO⁺ ions in the E region:

(1) Increase the NO density at low heights, to increase the conversion of O₂⁺ to NO. Approximate agreement with the Rocket data of Table 1, at a height of 110 km and

$\chi < 80^\circ$, is obtained if NO densities are increased by a factor of about 2 at $F_{10.7} = 140$ (and a factor of 3 at $F_{10.7} = 70$). These changes reduce the calculated values of N_mE by about 7%.

(2) Increase the rate constants for the conversion of O₂⁺ to NO⁺. This has basically the same effect as (1). Reaction rates must be increased by a factor of 2–3, giving a decrease of about 7% in calculated values of N_mE . Other reactions that produce NO⁺ are negligible at 110 km, because of the low densities of O⁺ and N⁺.

(3) Increase the direct production of NO⁺ near 110 km. The peak absorption of Ly α can be raised to this height by increasing the ionisation cross-section for NO. The change required is a factor of several hundred, and gives an increase of about 20% in N_mE .

(4) Decrease the loss rate for NO⁺. Loss occurs only through direct recombination, with a rate constant just over twice that for the direct recombination of O₂⁺. Decreasing this rate by a factor of 2 gives adequate NO⁺ at 110 km, for $F_{10.7} = 140$. It also gives too high a proportion of NO⁺ (about 70%) at heights near 150 km, and an unacceptable increase of 35% in N_mE .

Errors of 100% or more in the different rate constants seem unlikely, and the data in Fig. 1a appear to rule out a similar increase in equinoctial NO densities. Errors of 100% in the rocket measurements of NO⁺, at low heights, also seem unlikely – although the disparity between the independent rocket results at $\chi = 57^\circ$ and $\chi = 60^\circ$ in Table 1 suggests that further experimental data are

necessary. Perhaps the solution of this problem will involve several small adjustments. These could produce changes of the order of 5% in calculated values of N_mE , and in the width and depth of the E-F1 valley region.

4.2 Electron density

Calculated summer day profiles are compared with the experimentally based IRI-90 value of N_mE in Fig. 5. When secondary ionisation is omitted we get the results shown by the left-most broken line, with a peak (E-layer) density 30% less than the IRI value for these conditions. The continuous line, including a full allowance for photoelectrons and ionising radiations down to 25 Å (as described in Titheridge, 1996), gives much better agreement. The EUVAC radiation model uses the F74113 reference spectrum with fluxes increased by a factor of 2 from 150–250 Å, and by a factor of 3 at wavelengths $\lambda < 150$ Å, to improve agreement with measured photoelectron fluxes (Richards *et al.*, 1994). If this latter factor is increased to 4.0, giving an additional 33% increase in the fluxes at $\lambda < 150$ Å, we get the profile shown by the heavy broken line in Fig. 5. This is now only 3% below the IRI value for these summer conditions. Increasing the EUV fluxes by 18% at all wavelengths gives a similar result, as shown by the fine broken line.

With no adjustment to the EUVAC radiations, agreement with the IRI value of N_mE can be obtained by ignoring the presence of neutral NO; this gives the profile shown by the dotted line in Fig. 5. This approach does not seem acceptable, however, since the presence of substantial amounts of NO seems well-established. Agreement can also be obtained if the production of secondary ionisation is increased by about 60%. This can just be achieved by reducing the electron excitation cross-sections for O₂ and N₂ by a factor of 4 or more (Titheridge, 1996), but this also conflicts with current measurements.

Figure 6 shows the changes that can be obtained by altering the radiation models and ionisation constants. The heavy continuous line is the present result, as in Fig. 5. Changing to the earlier photoionisation cross-sections of Richards and Torr (1988) gives the result shown by the thin continuous line. This agrees reasonably well with the value of N_mE from the IRI standard. The increased ionisation near 107 km is, however, obtained at the expense of a large decrease at greater heights, giving an E-F valley that is wider (27 km) and deeper (22%) than normally expected. The thick chain line uses the modified Hinteregger radiations (with the same radiation bands, as described in Sect. 2, and fluxes doubled at $\lambda < 250$ Å as in Richards and Torr, 1988). This gives densities matching the IRI value of N_mE very closely, but again the E-F valley is rather too large. Use of Hinteregger radiations with the older cross-sections gives a large increase in N_mE and far too large a valley region, as shown by the fine chain line in Fig. 6. Thus acceptable values for both the peak density in the E region, and the valley between the E and F1 regions, are most readily obtained by using the EUVAC radiation model (preferably with a 33% increase at $\lambda < 150$ Å), in

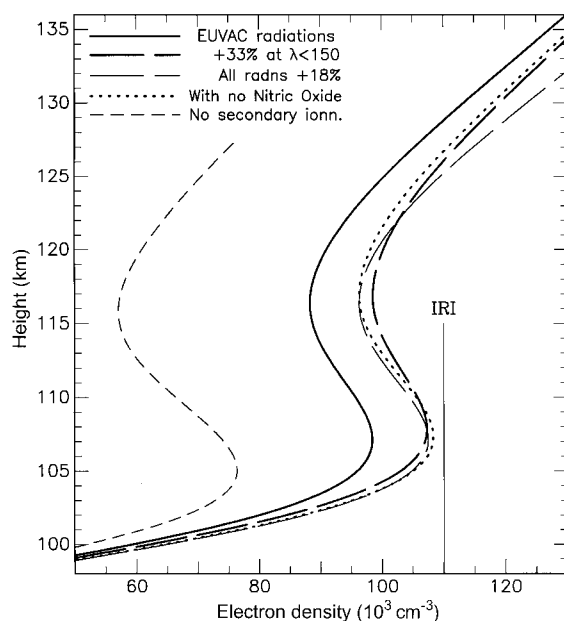


Fig. 5. E-region profiles calculated for summer conditions at 40°N, with $\chi = 60^\circ$ and $F_{10.7} = 120$. All curves use the EUVAC radiation model of Richards *et al.* (1994), and current values for the ionisation cross-sections (from Fennelly and Torr, 1992)

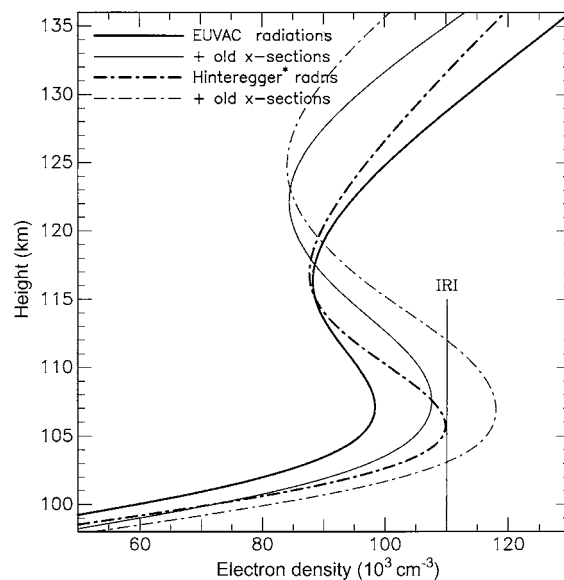


Fig. 6. E-region profiles calculated for summer noon conditions, as in Fig. 5. Continuous lines use the EUVAC radiation model, with 'normal' (heavy line) or reduced (fine line) ionisation cross-sections. Chain lines give corresponding results for the modified Hinteregger radiations of Richards and Torr (1984, 1988)

conjunction with recent values for the photoionisation cross-sections.

Comparisons between model results and observed electron densities in the E region have also been made by Buonsanto (1990) and Buonsanto *et al.* (1992, 1995). These use data obtained with the Millstone Hill radar, and so relate to individual occasions rather than the mean

ionosphere used in the present work. In the most recent study (Buonsanto *et al.*, 1995) plotted results show that use of the older ionisation cross-sections, instead of the more recent values from Fennelly and Torr (1992), gives an increase of about 8% in N_mE . This compares well with the increase of 9% in Fig. 6. There is also a similar increase in valley width, from 17 to 27 km in Fig. 6 and from 18 to 30 km in Fig. 2 of Buonsanto *et al.* (1995) (using EUV fluxes from rocket data).

Figures 3 to 6 of Buonsanto *et al.* (1995) show the effect of changing from the EUVAC radiation model to, among others, the modified Hinteregger model. This gave increases in N_mE of 10%, 20%, 23% and 29% under different conditions. The mean change is much larger than the increase of 12% found in Fig. 6 of the present work. Buonsanto *et al.* note, however, that their ionospheric model gives insufficient secondary ionisation with the EUVAC radiations. This is because it uses fixed ratios of secondary- (P_e) to-primary (P_i) ionisation, as a function of optical depth, based on the calculations of Richards and Torr (1988) using the earlier flux model. The EUVAC model has larger fluxes in all bands that produce secondary ionisation, and less in other bands. This gives a significant increase in P_e/P_i , that is obtained automatically from the approach used in the present work (Sect. 2). Thus the smaller increase found here, on changing from EUVAC to the Hinteregger radiations, is due to the higher secondary production obtained with the EUVAC spectrum. Reducing this secondary production by 35% gives about the same mean P_e/P_i ratio as for the Hinteregger radiations, and a decrease of 8% in N_mE . Changing from this result to one using the Hinteregger radiations then gives an increase of 21% in N_mE , in full agreement with the mean increase found by Buonsanto *et al.* (1995).

Other ionospheric data provide support for higher fluxes in the short radiation bands, as in the EUVAC model. Only wavelengths less than 150 Å, or longer than 1000 Å, produce significant amounts of ionisation at heights near 110 km. Calculations show that, for the EUVAC model, short wavelengths produce 62% of the ionisation at $F_{10.7} = 60$, 66% at $F_{10.7} = 100$ and 69% at $F_{10.7} = 200$. These figures agree well with the results of eclipse measurements by Bomke *et al.* (1970), who found that 68% of the ionisation was from the short-wavelength region. For the modified Hinteregger radiations, short wavelengths produce only about 45% of the total E-region ionisation, for all values of $F_{10.7}$. This is significantly less than the experimental result, and suggests that the factor-of-2 increase used at $\lambda < 250$ Å, in the ‘modified’ model, is insufficient.

5 Changes with solar flux

In both the EUVAC and Hinteregger radiation models, the EUV fluxes are a function of the daily $F_{10.7}$ index and the average value ($F_{10.7A}$) over an interval of 81 days centred on the current date. All calculations in this paper take $F_{10.7A} = F_{10.7}$, so that results apply to long-term variations in solar flux. The two parameters ($F_{10.7}$ and $F_{10.7A}$) are given equal weights in the EUVAC model.

Day-to-day fluctuations in solar activity, about a constant mean level, will then produce changes in EUV that are just half as large as for long-term variations.

In both radiation models the intensities of all radiations increase linearly with the 10.7-cm flux, since they are obtained by linear interpolation between data sets at $F_{10.7} = 80$ and 200 (Richards *et al.*, 1994). Between these sets, the intensities of different bands increase by factors of 1.4 to 4. Taking only those radiations that ionise below 135 km, and weighting each band by the amount of ionisation it produces, gives a mean increase by a factor of 1.88. Thus for the EUVAC radiations, at E-region heights, the ionisation production rate Q varies as $F_{10.7} + 56$. Normal E-region theory assumes quadratic recombination, giving $dN/dt = Q - \alpha N^2$ where α is the recombination coefficient. Time-constants near the E peak are only about 2 min, so that densities are always close to the equilibrium value. The density at the peak of the E-layer is then proportional to the square root of the production rate, giving

$$N_mE = A(F_{10.7} + B)^{0.5}, \quad (12)$$

where A is some constant, and $B = 56$ for the EUVAC radiation model and simple quadratic recombination.

Model calculations for noon equinox conditions, using a fixed atmospheric temperature and composition with no NO, give a variation of N_mE with $F_{10.7}$ that corresponds to $B = 53$ in Eq. 12. Thus densities increase slightly faster than predicted by simple theory, indicating that a small part of the recombination follows a linear (rather than quadratic) form. Including a fixed amount of NO (corresponding to $F_{10.7} = 100$, at noon) gives a slightly increased loss rate for O_2^+ , through the charge-exchange reaction $O_2^+ + NO \rightarrow O_2 + NO^+$. This is followed by recombination of NO^+ , with a rate coefficient about twice that for the direct recombination of O_2^+ . The first (charge exchange) step of this process introduces some dependence on linear loss processes. Calculated values of N_mE then vary more rapidly with $F_{10.7}$, giving $B = 45$ in Eq. 12.

Calculations with no NO, but allowing the atmosphere to vary with $F_{10.7}$ (as given by the MSIS model, for equinox conditions) give $B = 60$ in Eq. 12. Thus normal composition changes, as given by the MSIS86 atmospheric model, slightly reduce the variation of N_mE with solar activity. When a varying NO is also included we get $B = 95$, since the increased NO densities near solar maximum give larger loss rates and a larger reduction in N_mE .

Figure 7 shows the calculated variation of N_mE with solar flux, for summer noon conditions at a latitude of 40°N. With a solar zenith angle of 16.5°, changes under these conditions will reflect most directly the changes in the ionising radiation. Results are plotted against $(F_{10.7} + 40)^{0.5}$, since this gives an almost linear variation for most data sets and is accurately linear for the experimentally based IRI values. The continuous line in Fig. 7 is from the full atmospheric model, giving a variation corresponding to $B = 110$ in Eq. 12. When NO is neglected (dotted line) the model values correspond to $B = 68$ – still slightly greater than the value of 56 expected for simple

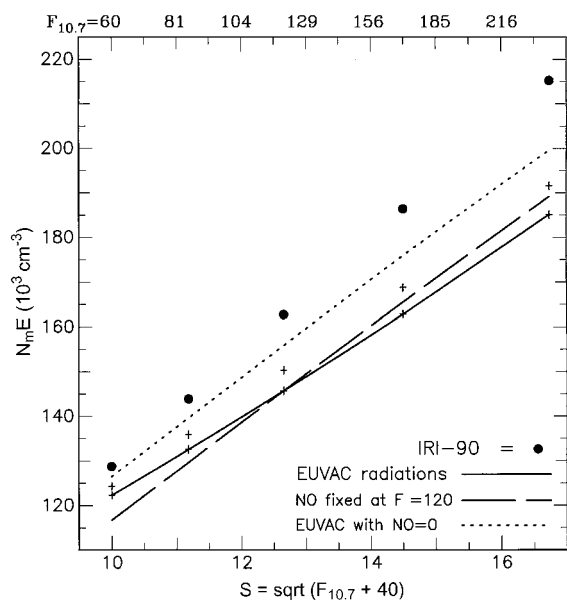


Fig. 7. The electron density at the peak of the E-layer ($N_m E$) plotted as a function of $(F_{10.7} + 40)^{0.5}$, where $F_{10.7}$ is the 10.7-cm solar flux (top scale). All results are for summer noon conditions at a latitude of 40°N , with $\chi = 16.5^\circ$. Solid dots represent mean observed values for these conditions, from the IRI-90 empirical model. The continuous line is from calculations using the EUVAC radiation model. Broken and dotted lines are obtained when the changes of NO density with $F_{10.7}$ are suppressed. Points marked + are with half the normal NO

quadratic recombination. The results plotted as + in Fig. 7 are obtained when the NO densities are halved. These points fall roughly halfway between the solid and dotted lines, showing that the variation of $N_m E$ with NO density is approximately linear.

The fastest change of $N_m E$ with $F_{10.7}$ is obtained by removing the increase of NO near solar maximum, and giving increased emphasis to linear recombination processes. These requirements are both met by using a fixed NO density. Results when the NO density is held constant at the value corresponding to $F_{10.7} = 120$ are shown by the broken line in Fig. 7. This has a slope corresponding to $B = 49$ in Eq. 12. Use of fixed NO densities corresponding to $F_{10.7} = 180$ gives $B = 46$, but this requires an unacceptably large NO density at solar minimum and gives too-small values of $N_m E$ at all times.

Our best current estimate of mean observed values of $N_m E$, under different conditions, comes from the IRI-90 ionospheric model (Bilitza, 1990). The expressions for $N_m E$ in this model are derived from an analysis of a large experimental data base, by Kouris and Muggleton (1973a, b), and provide a good representation of mean observed values as a function of solar zenith angle, latitude, season and solar flux. The solid dots in Fig. 7 show the values of $N_m E$ given by the IRI-90 model for summer noon conditions at 40°N , with $\chi = 16.5^\circ$. The plotted values are for $F_{10.7} = 60, 85, 120, 170$ and 240 . At solar minimum these points are only 5% above the full model results (solid line). At $F_{10.7} = 170$, however, the IRI values are 16% above the full model. The slope of the IRI

variation corresponds to $B = 40.4$ in Eq. 12, showing an appreciably faster change than in any model results using the EUVAC radiations.

The change of $N_m E$ with $F_{10.7}$, as given by the IRI-90 model, is larger than that which would be obtained from the EUVAC radiation model assuming that all loss is quadratic (giving $B = 56$). Even with an artificially large and constant value for the assumed density of NO, calculations using the EUVAC model give $B = 46$. This corresponds to a solar-cycle increase that is significantly below the experimental value. Other possible changes in the production or loss mechanisms near solar maximum seem little help. Increased electron temperatures could reduce the recombination rates for O_2^+ , N_2^+ and NO^+ , but an increase of 100% in $T_e - T_n$ gives an increase of only 3.5% in $N_m E$. Alternatively the direct production of O_2^+ could be increased by a larger proportion of O_2 in the atmosphere, near solar maximum. Increasing the O_2 densities by 40%, and decreasing N_2 by 10% to keep the same overall density, gives an increase of 6% in $N_m E$. This is barely sufficient to explain the changes at solar maximum, and composition errors of this size in the MSIS86 model (at solar maximum only) seem unlikely. Buonsanto (1990) has shown that an overall decrease in neutral densities will give increased electron densities. For a 25% decrease in the density of all components, the present calculations give an increase in $N_m E$ which varies from 2% at solar minimum to 4% at solar maximum. These changes, at a height of 110 km, are appreciably less than the changes of 5–10% found by Buonsanto at 180 km, and are not sufficient to explain the too-small values of $N_m E$ near solar maximum.

Some changes in E-region chemistry near solar maximum cannot be ruled out. As noted in Sect. 4.1, current modelling calculations give ratios NO^+/O_2^+ which appear significantly less than some experimental data in the lower E region. This suggests that our knowledge of E-region chemistry is incomplete. Introduction of new reactions, or new temperature variations, could result in an increased solar-cycle variation in calculated values of $N_m E$.

A more likely way to provide increased ionisation near solar maximum is through revision of the EUV model. An increase of 20% in the solar maximum reference spectrum used in the EUVAC model (at $F_{10.7} = 200$) gives results shown by the broken line in Fig. 8. This matches the slope of the IRI variation quite accurately, giving $B = 39$ in Eq. 12. These results include the full NO allowance, and give values of $N_m E$ which are about 6% below the IRI values throughout the solar cycle.

The chain line in Fig. 8 shows the variation calculated using the modified Hinteregger radiations (Richards and Torr, 1988). These results match the IRI values quite closely, at all stages of the solar cycle, with an error that decreases from -3% at $F_{10.7} = 60$, to 0% at $F_{10.7} = 230$. Thus the solar-cycle increase used in the Hinteregger model slightly exceeds that required to match the observed changes in $N_m E$. This occurs because the H-Ly β radiation, that provides most O_2^+ ionisation in the E region, has a solar cycle increase that is 27% larger in the Hinteregger data than in the EUVAC model. The Hinteregger spectrum does, however, give E-F region valleys

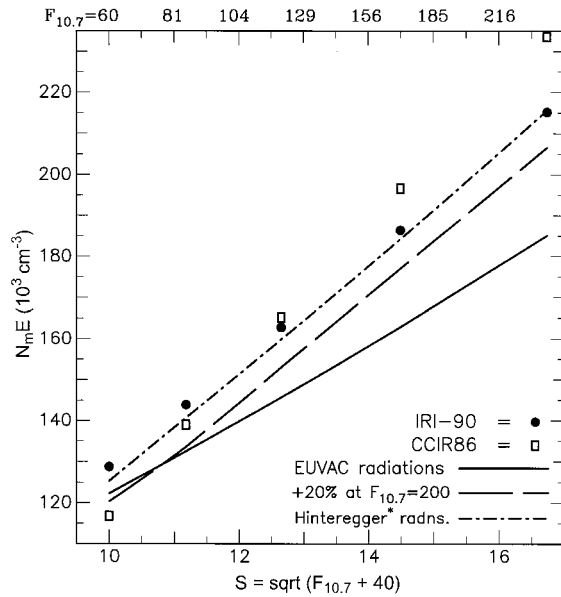


Fig. 8. Changes in $N_m E$ obtained with different radiation models, using the full atmospheric model (with varying NO). The EUVAC model with a 20% increase in fluxes at high solar activity gives the broken line. The chain line gives results obtained using the Hinteregger radiations

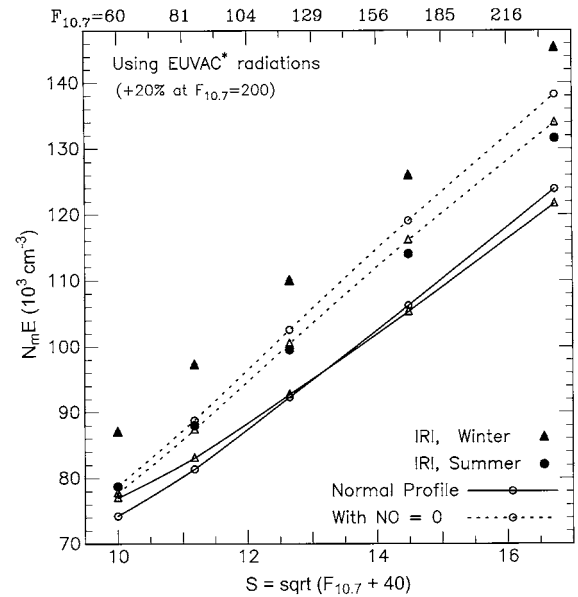


Fig. 9. The variation of $N_m E$ with solar flux for summer (circles) and winter (triangles). Results are for a latitude of $40^\circ N$, at a constant solar zenith angle $\chi = 65^\circ$. Solid symbols are from the IRI empirical model. Continuous and dotted lines are from model calculations with and without the inclusion of NO

which are appreciably too large throughout the solar cycle (as in Fig. 6). Thus optimum agreement with observations requires a spectrum similar to that used in the EUVAC model, with fluxes increased near solar maximum to match the changes given by the Hinteregger data.

The IRI-90 model corresponds to the CCIR78 model, based on the E-region studies of Kouris and Muggleton (1973a, b). For CCIR use this was later replaced by the simpler CCIR86 model, which ignores seasonal or latitude changes and assumes that ionospheric production varies as $F_{10.7}$. Thus the CCIR86 model uses Eq. 12 with $B = 0$. Values of $N_m E$ calculated from this model are shown as squares in Fig. 8. While they agree with the IRI values at $F_{10.7} \approx 108$, the solar variation is much too large. The CCIR86 model could be greatly improved by substituting $0.73(F_{10.7} + 40)$ for $F_{10.7}$.

6 Seasonal changes

Early studies of the E region revealed a seasonal anomaly at mid-latitudes, with $N_m E$ 5–15% higher in winter than in summer (Appleton, 1963; Muggleton, 1972). A detailed analysis by Kouris and Muggleton (1973a, b) used monthly median data from 45 stations, averaged over a full sunspot cycle. Data were corrected for changes in the solar zenith angle, and in the sun-earth distance. Results showed mean values of $N_m E$ that were approximately constant at the equator and in winter, but decreased by about 7% in summer. This change is incorporated in the IRI-90 model, as shown by the solid circles (summer) and triangles (winter) in Fig. 9.

Relative to the summer values of $N_m E$, the IRI model gives an increase in winter of about 2%, 10% and 12% at

latitudes of 20° , 40° and 60° , respectively. The IRI data plotted in Fig. 9, for a latitude of $40^\circ N$, show a constant increase of 10.4% from summer to winter. When the presence of NO is ignored, model calculations give the dotted lines that show a decrease of 1.0% (solar minimum) to 2.4% (solar maximum) in winter. This is caused by composition changes in the MSIS86 atmospheric model. In the southern hemisphere, these changes give an increase in winter, of 2.9% (solar minimum) to 3.6% (solar maximum). Thus the changes in the MSIS86 atmospheric model are basically annual. They are larger and in the right direction to produce the observed seasonal anomaly in $N_m E$ in the southern hemisphere, but are too small by a factor of about 3.

At solar minimum, in both hemispheres, inclusion of NO decreases the summer values of $N_m E$ by about 6%. In winter the change is only 1%, since the NO density is only about one-quarter of the summer value (Fig. 1b). As a result, the presence of NO gives a small seasonal anomaly in the northern hemisphere, with $N_m E$ increasing by about 4% from summer to winter (at a fixed zenith angle). In the southern hemisphere, the annual composition changes in the MSIS86 model combine with the NO variations to produce a seasonal anomaly of about 8%, which is close to the observed value.

Near solar maximum, the inclusion of NO gives a reduction of 11% in the summer values of $N_m E$, as shown in Fig. 9. In winter the decrease in $N_m E$ is 9%, only slightly less than in summer. This is because the satellite data used for the present model give approximately the same absolute change in NO from winter to summer at all levels of solar activity (Fig. 1b). Thus the summer increase in NO is too small to explain the seasonal anomaly in $N_m E$ near solar maximum.

The seasonal anomaly is observed in both hemispheres, so it cannot be caused by changes in the solar radiation. Changes in atmospheric composition or temperature also seem inadequate to explain the observations, as discussed above. This leaves movements as a possible cause. Electric fields, or winds in the neutral atmosphere, can cause a vertical drift of ionisation at mid-latitudes. If the drift velocity U changes with height, we get an additional production term $dQ = \text{div}(N \cdot U)$ in the continuity equation. At the height of the peak this reduces to $dQ = N \cdot dU/dh$. Assuming a quadratic loss process in the E-layer, the normal relation $Q = \alpha N^2$ then gives the change in peak density, due to the vertical drift, as

$$dN = (1/2\alpha) dU/dh. \quad (13)$$

The rate coefficient α , for direct recombination of O_2^+ , is about $1.5 \times 10^{-7} \text{ cm}^3 \text{ s}^{-1}$. If the vertical drift U changes by 10 m s^{-1} in a vertical distance of 10 km, we get $dN = 3000 \text{ cm}^{-3}$ from Eq. 13. For a typical daytime E-layer with $N_m E \approx 1 \cdot 10^5 \text{ cm}^{-3}$, this is a change of 3% in $N_m E$. Allowing for the fact that over 30% of the daytime recombination is via additional loss processes (such as charge exchange with N or NO, to give NO^+), reduces the expected change in $N_m E$ to less than 2%. This is confirmed by full model calculations. A vertical drift that changes by 10 m s^{-1} in 10 km alters $N_m E$ by 1.8% when the presence of NO is ignored, and by 1.6% when it is included. The percentage change is somewhat larger near sunrise and sunset since, as shown by Eq. 13, the absolute change dN is independent of N .

At mid-latitudes, the above vertical drifts correspond to a horizontal (meridional) wind that changes by least 20 m s^{-1} between heights of 100 and 110 km. Normal ionospheric winds (reviewed in Titheridge, 1995) show a height variation of about half this amount, in a direction that would decrease $N_m E$ by up to 1% near noon. To obtain a 10% difference between summer and winter would require a regular seasonal change in the wind shear through about ten times the mean value. There is no variation of this type in current models or observations. Since the wind shears cannot be maintained over a large height range, any such effect would be accompanied by large seasonal changes in the size of the E-F1 valley region, which have not been observed.

Vertical movements of ionisation can also be caused by horizontal electric fields, and fields associated with the equatorial electrojet have been postulated as a cause of the seasonal anomaly in $N_m E$ (Kouris and Muggleton, 1973b). This was based partly on the result that, for a simple Chapman layer, a steady vertical drift will produce some change in $N_m E$. No numerical results were given, but the simplified equation shown gives a change of about 10% in $N_m E$ for a vertical drift $U = 30 \text{ m s}^{-1}$. Full model calculations show a change of only 1.1% in $N_m E$ for a steady drift of this size, and unrealistically large drifts are required to obtain a 10% change in $N_m E$. This leaves the question as to whether electric fields can produce a large vertical drift gradient in the E region. The results of Richmond *et al.* (1980) show vertical drifts at mid-latitudes of $5\text{--}30 \text{ m s}^{-1}$, at F-region heights, with day-to-day

variations of around 100%. These drifts apply to an entire field line, so there can be no large seasonal changes. Latitude variations also seem inadequate to give a consistent change of 10 m s^{-1} in a vertical distance of only 10 km, in the E region. Thus in the absence of full quantitative calculations, it appears unlikely that electrojet fields could give sufficiently large, regular variations in the vertical drifts to account for the E-region seasonal anomaly.

These difficulties make it appropriate to re-examine the possibility of obtaining a larger seasonal variation from changes in the NO density. The mean summer and winter curves of Fig. 1b, obtained as fits to the plotted data, are rather unsatisfactory from a physical viewpoint. As the solar radiation increases, we would expect a similar increase in the mean NO densities in both winter and summer. Production is from direct or indirect dissociation of N_2 , and this gas has no large seasonal or solar-cycle changes in the E region. The loss processes depend primarily on neutral $N(^4S)$, which also has little seasonal or solar variation in the MSIS86 model (although these data may be unreliable in the E region, as noted in Sect. 3.1). The β -type loss should give NO densities that vary in the same way as the solar radiation. This is confirmed in calculations by Fuller-Rowell (1993), who used a one-dimensional, globally averaged model of the thermosphere to determine the changes with solar activity. Results showed a change in NO densities by a factor of 4, for $F_{10.7}$ increasing from 70 to 190. This agrees accurately with the change in Fig. 1a, defined by mean SME measurements over the equator.

At $F_{10.7} = 70$, Fig. 1b gives an increase by a factor of 2.3 from winter to summer. This seems about right. Multiplying the value of $\cos \chi$ at noon by the number of hours from sunrise to sunset, to give a rough measure of the total solar input, gives a summer-to-winter ratio of 2.3 at a latitude of 30° . At $F_{10.7} = 190$, however, the curves in Fig. 1b give a summer increase by a factor of only 1.24. This change seems far too small, unless there are large seasonal changes in atmospheric composition, that vary with solar activity. NO time-constants are too short to allow horizontal mixing between hemispheres, so we would expect the summer/winter ratio to be roughly constant throughout the solar cycle.

To obtain a more nearly constant ratio, Eq. 2 can be modified to

$$D_0 = A + B(F_{10.7} - 100) - 0.0008(F_{10.7} - 100)^2 \times 10^6 \text{ cm}^{-3}. \quad (14)$$

where $A = 14.8 + 0.1s \cdot \phi + C$, $B = 0.22 + 0.026C$ and C is a correction term given by $C = 0.05s \cdot \phi$. Setting $C = 0.0$ gives the original form of Eq. 2. For latitudes of 30°N and 30°S , in summer and winter, Eq. 14 gives the curves shown as dotted lines in Fig. 1b. The seasonal change in NO density, at a latitude of 30° , is now a factor of 2.2 at $F_{10.7} = 80$ and a factor of 1.8 at $F_{10.7} = 180$. The dotted lines in Fig. 1b provide a rather poor fit to the SME data at $F_{10.7} > 120$, particularly in winter, but this must be accepted if we wish to avoid a greatly reduced seasonal change near solar maximum. The maximum fit error of about 20% may still be acceptable, since there are

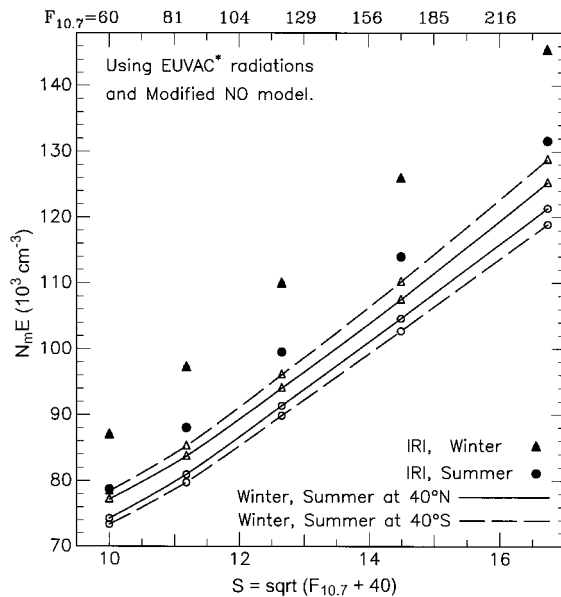


Fig. 10. Calculated values of $N_m E$, for the same conditions as in Fig. 9, using a modified model for the seasonal changes in NO. Continuous and broken lines are for latitudes of 40°N and 40°S , respectively

large day-to-day variations in NO densities and the SME data may not accurately reflect mean conditions.

Calculations using this revised NO model give the values of $N_m E$ plotted in Fig. 10. Results obtained for latitudes of 40°N and 40°S are shown as continuous and broken lines, respectively. These are for a low level of magnetic activity ($A_p = 10$) in the MSIS86 model, and a longitude of 10°E . Similar results are obtained at other longitudes. There is now a significant seasonal anomaly in both hemispheres, at all stages of the solar cycle. At 40°N , the calculated winter values of $N_m E$ are 3.0–3.8% above the summer values at all times. At 40°S , where the composition changes in the MSIS86 model aid the winter increase, we get a seasonal anomaly of 7% at solar minimum and 8% at solar maximum. This is still less than the change of 10.4% in the IRI data. It does suggest, however, that the seasonal anomaly in $N_m E$ may be caused by a number of different effects with changes in atmospheric composition, and the NO density in particular, playing a large part.

Figure 10 is calculated using the EUVAC radiation model with fluxes increased by 20% at $F_{10.7} = 200$, as for Fig. 9. With the increased NO densities in summer, model values of $N_m E$ now lie 7–10% below the IRI values. In winter the difference is 12–15%. These differences could be removed by a mean increase of 20–25% in the EUV fluxes. Since current models differ by much more than this, in many regions, it seems possible that improved EUV models could lead to agreement with observed values of $N_m E$.

7 Conclusions

Recently-available data on the density of NO in the upper atmosphere, under different conditions, is used to con-

struct a physically reasonable model for the diurnal, seasonal and solar-cycle changes in this gas. The height variation is represented by a β -Chapman layer, with a peak near 110 km and a near-constant scale height. The peak density decreases exponentially at night, with a time-constant of 5–6 h. There is a rapid increase at sunrise, and a maximum near 14 h which is typically about seven times the presunrise minimum. At a latitude of 40° , and $F_{10.7} = 120$, daytime densities increase by about 50% from winter to summer. Data from the SME satellite indicate that this change is larger at solar minimum and less at solar maximum. Near equinox, mean densities change by a factor of about 4 over the solar cycle ($F_{10.7} = 70$ to 190). The presence of NO in the E region increases the loss rates for O_2^+ , reducing $N_m E$ by about 5% at solar minimum and 12% at $F_{10.7} = 240$.

For summer noon conditions, and medium levels of solar activity, profile calculations using the NO model and a full allowance for secondary ionisation (with EUV radiations down to 50 Å) give values of $N_m E$ that are about 10% below observed values. About 66% of the E region ionisation is produced by radiations with $\lambda < 150$ Å. Flux measurements at these wavelengths are subject to appreciable uncertainties, and the EUVAC data include a correction factor of 3 for this region. Increasing this factor to 4 gives a good match with observed summer noon values of $N_m E$, at $F_{10.7} = 120$.

Agreement with the IRI values of $N_m E$, for summer noon conditions at $F_{10.7} = 120$, can also be obtained by (i) use of older values for the ionisation cross-sections; (ii) use of the Hinteregger radiations (increased by a factor of 2 at $\lambda < 250$ Å); or (iii) ignoring the presence of NO. The last alternative seems unacceptable, since the presence of significant amounts of NO is well-established; (i) and (ii) seem undesirable since they ignore the newer estimates of radiation intensities and cross-sections, and give valleys between the E and F1 layers that appear too large. Changes in the neutral wind appear much too small, and in the wrong direction, to give a useful increase in $N_m E$ (Sect. 6).

Calculations using the modified Hinteregger radiations give summer values of $N_m E$ that agree closely with observed data at all stages of the solar cycle. The larger values of $N_m E$ obtained from this model come from a change in the relative amount of ionisation at different heights, giving decreased densities at heights above 110 km. The result is a large valley between the E and F regions which is appreciably deeper and wider than is normally expected. Thus the spectrum given by the Hinteregger model seems incorrect, although the solar-cycle changes provide a good fit to observed E-region densities.

In the newer EUVAC model, the shape of the EUV spectrum gives valleys that agree well with most observations. The increase in the EUV fluxes near solar maximum does, however, seem insufficient to produce the observed increase in $N_m E$, with any reasonable adjustments to atmospheric parameters. The solar-cycle change in the H-Ly β line, that produces most O_2^+ ionisation in the E region, is 22% less than in the Hinteregger data. It appears that parts of the high-flux spectrum F79050N, incorporated in the EUVAC model, should be increased by 20% or more to reflect mean conditions at solar

maximum. The same result can be achieved by increasing the fluxes at $\lambda < 150 \text{ \AA}$ by 33%, for the F79050N spectrum. E-region densities calculated from the EUVAC model then show a solar-cycle change that agrees closely with the IRI model.

These results are for summer conditions, with the sun nearly overhead (at $\chi = 16.5^\circ$). The IRI model gives an increase of 10.4% in $N_m E$, from summer to winter, for a fixed solar zenith angle and a latitude of 40° . This change is not reproduced in the model calculations. Normal variations in the MSIS86 model atmosphere produce a summer-to-winter change in $N_m E$ of about -1% at a latitude of 40°N , and $+2\%$ at 40°S . Seasonal variations in NO densities produce a summer to winter change in $N_m E$ of about $+5\%$ near solar minimum, giving an overall increase in winter of 3–4% at 40°N and 7% at 40°S . This is sufficient to explain about half of the observed seasonal anomaly in $N_m E$. Near solar maximum, the relative change in NO densities is much less and gives a winter increase of only about 2% in $N_m E$.

Possible changes due to the effect of varying winds or electric fields seem much too small to produce a 10% increase in $N_m E$ in winter. It is therefore suggested that the seasonal variation in NO densities near solar maximum, as obtained from current satellite data, may not accurately reflect mean conditions. Simple calculations of the total solar irradiance suggest that NO densities should double in summer, at a latitude of 30° . Current data suggest a summer/winter ratio of 2.3 at solar minimum but only 1.2 at solar maximum. Allowing errors of $\pm 20\%$ in the solar-maximum data gives a revised model with a seasonal change of 1.8 at this time. Calculations then give a seasonal anomaly of 3–4% at 40°N , and 7–8% at 40°S , at all stages of the solar cycle. Thus it seems that the anomaly may have several causes, with composition changes (particularly in NO) contributing a major part.

Acknowledgements. Computer programs and data for the MSIS86 model (by A. E. Hedin) and the IRI-90 model (organised by D. Bilitza) were provided by the National Space Science Data Center, through the World Data Center A for Rockets and Satellites, Greenbelt, Maryland.

Topical Editor D. Alcaydé thanks J.-C. Gérard and P. Richards for their help in evaluating this paper.

References

- Appleton, E. V., A seasonal anomaly in the ionospheric E-layer, *J. Atmos. Terr. Phys.*, **25**, 577–579, 1963.
- Barth, C. A., Reference models for thermospheric NO, *Adv. Space Res.*, **10**, (10)103–115, 1990.
- Barth, C. A., W. K. Tobiska, D. E. Siskind, and D. D. Cleary, Solar-terrestrial coupling: Low-latitude thermospheric nitric oxide, *Geophys. Res. Lett.*, **15**, 92–94, 1988.
- Bilitza, D., International Reference Ionosphere 1990, Report 90-22, National Space Science Data Center, World Data Center A for Rockets and Satellites, Code 930.2, Goddard Space Flight Center, 1990.
- Bomke, H. A., H. A. Blake, A. K. Harris, and D. J. Sheppard, An eclipse study of soft-X-ray distribution over the sun and of the relative contributions of X rays and UV to E-layer formation, *J. Geophys. Res.*, **75**, 6980–6990, 1970.
- Buonsanto, M. J., A study of the daytime E-F1 region ionosphere at mid-latitudes, *J. Geophys. Res.*, **95**, 7735–7747, 1990.
- Buonsanto, M. J., S. C. Solomon, and W. K. Tobiska, Comparison of measured and modelled solar EUV flux and its effect on the E-F1 region ionosphere, *J. Geophys. Res.*, **97**, 10513–10524, 1992.
- Buonsanto, M. J., P. G. Richards, W. K. Tobiska, S. C. Solomon, Y.-K. Tung, and J. A. Fennelly, Ionospheric electron densities calculated using different EUV flux models and cross-sections: Comparison with radar data, *J. Geophys. Res.*, **100**, 14569–14580, 1995.
- Danilov, A. D., and V. K. Semenov, Relative ion composition model at midlatitudes, *J. Atmos. Terr. Phys.*, **40**, 1093–1102, 1978.
- Fennelly, J. A., and D. G. Torr, Photoionisation and photoabsorption cross sections of O, N₂, O₂, and N for aeronomic calculations, *At. Data Nucl. Data Tables*, **51**, 321–363, 1992.
- Fesen, C. G., D. W. Rusch, and J.-C. Gérard, The latitude gradient of the NO peak density, *J. Geophys. Res.*, **95**, 19053–19059, 1990.
- Fuller-Rowell, T. J., Modelling the solar cycle change in nitric oxide in the thermosphere and upper mesosphere, *J. Geophys. Res.*, **98**, 1559–1570, 1993.
- Gérard, J.-C., and C. E. Noël, AE-D measurements of the NO geomagnetic latitudinal distribution and contamination by N + (5S) emission, *J. Geophys. Res.*, **91**, 10136–10140, 1986.
- Gérard, J.-C., C. G. Fesen, and D. W. Rusch, Solar cycle variation of nitric oxide at solstice, *J. Geophys. Res.*, **95**, 12235–12241, 1990.
- Gérard J.-C., V. I. Shematovich, and D. V. Bisikalo, Effect of hot N(4S) atoms on the NO solar cycle variation in the lower thermosphere, *J. Geophys. Res.*, **98**, 11581–11586, 1993.
- Hedin, A. E., MSIS-86 thermospheric model, *J. Geophys. Res.*, **92**, 4649–4662, 1987.
- Keneshea, T. J., R. S. Narcissi, and W. Swider Jr., Diurnal model of the E region, *J. Geophys. Res.*, **75**, 845–854, 1970.
- Kouris, S. S., and L. M. Muggleton, Diurnal variation in the E-layer ionisation, *J. Atmos. Terr. Phys.*, **35**, 133–139, 1973a.
- Kouris, S. S., and L. M. Muggleton, World morphology of the Appleton E-layer seasonal anomaly, *J. Atmos. Terr. Phys.*, **35**, 141–151, 1973b.
- Kuze, A., and T. Ogawa, Solar cycle variation of thermospheric NO: A model sensitivity study, *J. Geomagn. Geoelectr.*, **40**, 1053, 1988.
- Mitra, A. P., and P. Benerjee, Solar activity variation of $[\text{NO}^+]/[\text{O}_2^+]$ and $[\text{NO}^+]/[\text{O}^+]$ in E and F regions, Scientific Report No. 67, Radio Science Division, National Physical Laboratory, Delhi-12, India, August 1971.
- Muggleton, L. M., Regression-line studies of the E-region seasonal anomaly, *J. Atmos. Terr. Phys.*, **34**, 1385–1391, 1972.
- Richards, P. G., and D. G. Torr, Ratios of photoelectron to EUV ionisation rates for aeronomic studies, *J. Geophys. Res.*, **93**, 4060–4066, 1988.
- Richards, P. G., J. A. Fennelly, and D. G. Torr, EUVAC: A solar EUV flux model for aeronomic studies, *J. Geophys. Res.*, **99**, 8981–8992, 1994.
- Richmond, A. D., M. Blanc, B. A. Emery, R. H. Wand, B. G. Fejer, R. F. Woodman, S. Ganguly, P. Amayenc, R. A. Behnke, C. Calderon, and J. V. Evans, An empirical model of quiet-day ionospheric fields at middle and low latitudes, *J. Geophys. Res.*, **85**, 4658–4664, 1980.
- Rusch, D. W., J. C. Gérard, and C. G. Fesen, The diurnal variation of NO, N(2D), and ions in the thermosphere: a comparison of satellite measurements to model, *J. Geophys. Res.*, **96**, 11331–11339, 1991.
- Siskind, D. E., and D. W. Rusch, Nitric oxide in the middle to upper atmosphere, *J. Geophys. Res.*, **97**, 3209–3217, 1992.
- Smith, D. R., P. De, S. Adler-Golden, and C. Roth, Empirical correlations in thermospheric NO density measured from rockets and satellites, *J. Geophys. Res.*, **98**, 9453–9458, 1993.
- Stewart, A. I., and T. E. Cravens, Diurnal and seasonal effects in E region low-latitude nitric oxide, *J. Geophys. Res.*, **83**, 2453–2456, 1978.
- Swider, W., and T. J. Keneshea, The quiet sunrise E region: enhancements at high latitudes in winter due to increased nitric oxide, *J. Geophys. Res.*, **98**, 1725–1728, 1993.
- Titheridge, J. E., Aeronomic calculations of valley size in the ionosphere, *Adv. Space Res.*, **10**(8), 21–24, 1990.

Titheridge, J. E., Atmospheric winds calculated from diurnal changes in the mid-latitude ionosphere, *J. Atmos. Terr. Phys.*, **55**, 1637–1659, 1993.

Titheridge, J. E., Winds in the ionosphere – A review, *J. Atmos. Terr. Phys.*, **57**, 1681–1714, 1995.

Titheridge, J. E., A direct allowance for the effect of photoelectrons in ionospheric modelling, *J. Geophys. Res.*, **101**, 357–369, 1996.

Tobiska, W. K., Recent solar extreme irradiance observations and modelling: A review, *J. Geophys. Res.*, **98**, 18879–18894, 1993.

Torr, D. G., and M. R. Torr, Ionisation frequencies for solar cycle 21: Revised, *J. Geophys. Res.*, **90**, 6675–6678, 1985

Torr, M. R., D. G. Torr, T. Chang, P. Richards, W. Swift, and N. Li, Thermospheric nitric oxide from the ATLAS 1 and Spacelab missions, *J. Geophys. Res.*, **100**, 17389–17413, 1995.